Biochimica et Biophysica Acta 1852 (2015) 2484–2493

Contents lists available at ScienceDirect

Biochimica et Biophysica Acta

journal homepage: www.elsevier.com/locate/bbadis

HDAC6 inhibition induces mitochondrial fusion, autophagic flux and reduces diffuse mutant huntingtin in striatal neurons

Pedro Guedes-Dias [a,b], João de Proença [a], Tânia R. Soares [a], Ana Leitão-Rocha [a], Brígida R. Pinho [a], Michael R. Duchen [b], Jorge M. A. Oliveira [a,*]

[a] REQUIMTE/LAQV, Department of Drug Sciences, Faculty of Pharmacy, University of Porto, 4050-313 Porto, Portugal
[b] Department of Cell and Developmental Biology, University College London, London WC1E 6BT, UK

ARTICLE INFO

Article history:
Received 16 February 2015
Received in revised form 22 July 2015
Accepted 19 August 2015
Available online 21 August 2015

Keywords:
HDAC6
Mitochondria
Autophagy
Huntingtin
Huntington's disease
Neurodegeneration

ABSTRACT

Striatal neurons are vulnerable to Huntington's disease (HD). Decreased levels of acetylated alpha-tubulin and impaired mitochondrial dynamics, such as reduced motility and excessive fission, are associated with HD; however, it remains unclear whether and how these factors might contribute to the preferential degeneration of striatal neurons. Inhibition of the alpha-tubulin deacetylase HDAC6 has been proposed as a therapeutic strategy for HD, but remains controversial — studies in neurons show improved intracellular transport, whereas studies in cell-lines suggest it may impair autophagosome–lysosome fusion, and reduce clearance of mutant huntingtin (mHtt) and damaged mitochondria (mitophagy). Using primary cultures of rat striatal and cortical neurons, we show that mitochondria are intrinsically less motile and more balanced towards fission in striatal than in cortical neurons. Pharmacological inhibition of the HDAC6 deacetylase activity with tubastatin A (TBA) increased acetylated alpha-tubulin levels, and induced mitochondrial motility and fusion in striatal neurons to levels observed in cortical neurons. Importantly, TBA did not block neuronal autophagosome–lysosome fusion, and did not change mitochondrial DNA levels, suggesting no impairment in autophagy or mitochondrial clearance. Instead, TBA increased autophagic flux and reduced diffuse mHtt in striatal neurons, possibly by promoting transport of initiation factors to sites of autophagosomal biogenesis. This study identifies the pharmacological inhibition of HDAC6 deacetylase activity as a potential strategy to reduce the vulnerability of striatal neurons to HD.

1. Introduction

Huntington's disease (HD) is a fatal neurodegenerative disorder caused by polyglutamine (polyQ) expansion mutations in the huntingtin protein. Although ubiquitously expressed, mutant huntingtin (mHtt) induces selective neurodegeneration that is most harmful to striatal neurons [1]. There are several reports suggesting that mHtt can induce mitochondrial dysfunction [2–5], but it is not clear how that might contribute to preferential striatal neurodegeneration. One hypothesis is that striatal neurons are intrinsically vulnerable to mitochondrial dysfunction. Indeed, even without mHtt, striatal neurons show increased susceptibility to defects of oxidative phosphorylation [6], and to calcium-induced mitochondrial permeability transition [7] when compared to cortical neurons.

Abnormal mitochondrial dynamics including excessive mitochondrial fragmentation have been suggested to occur as early events in several neurodegenerative disorders, including HD [8,9]. A better understanding of mitochondrial fission and fusion, and of the regulatory factors involved, may lead to improved treatments and cures for these diseases. One open question is whether striatal and cortical neurons present intrinsic differences in their mitochondrial dynamics profile that may contribute to their differential vulnerability in HD. Concurrently, one notable challenge is to identify pharmacological strategies to counteract excessive mitochondrial fragmentation in HD [4,10].

HDAC6 is a cytosolic histone deacetylase presenting α-tubulin deacetylase and ubiquitin-binding activities [11]. HDAC6 inhibition was proposed as a therapeutic strategy for HD following evidence that it compensates intracellular transport deficits in HD models by increasing alpha-tubulin acetylation levels, which are decreased in HD patient brains [12,13]. However, targeting HDAC6 in HD is controversial since studies in cell lines suggest that HDAC6 is necessary for autophagosome–lysosome fusion [14], and also that HDAC6 mediates the clearance of mHtt [15] and damaged mitochondria [16], thereby predicting detrimental effects for HDAC6 inhibition in HD. Still, this prediction contrasts with data showing no evidence of brain abnormalities in HDAC6-knockout mice [17,18], thus failing to support a role for HDAC6 in autophagosome–lysosome fusion, which would be expected to impair autophagy and cause neurodegeneration [19]. It is

* Corresponding author at: Faculty of Pharmacy, University of Porto, Rua Jorge Viterbo Ferreira, 228, 4050-313 Porto, Portugal.
E-mail address: jorgemao@ff.up.pt (J.M.A. Oliveira).

http://dx.doi.org/10.1016/j.bbadis.2015.08.012
0925-4439/

therefore important to clarify whether pharmacological HDAC6 inhibition affects neuronal autophagy, and also the clearance of mitochondria and mHtt in neurons.

Primary cultures of striatal and cortical neurons are frequently used as an experimental model to explore the differential vulnerability in HD [7,20]. Here we used fluorescence live-imaging and molecular techniques to investigate whether these neuronal populations present intrinsic differences in mitochondrial motility and fission–fusion dynamics, and whether such dynamics are modulated by HDAC6 inhibition. We also investigate whether pharmacological HDAC6 inhibition affects neuronal autophagosome–lysosome fusion, and how it impacts autophagic flux, mitochondrial levels, and the proteostasis of wild-type and mutant huntingtin in striatal and cortical neurons.

2. Materials and methods

2.1. Plasmids and antibodies

Plasmids: mito-DsRed2 (mtDsRed; Michael Ryan, La Trobe University, Australia), mCherry-EGFP-LC3B (Jayanta Debnath, University of California, USA — Addgene 22418 [21]), EGFP-Htt^{ex1}Q23 and EGFP-Htt^{ex1}Q74 (David Rubinsztein, University of Cambridge, UK — Addgene 40261 and 40262 [22]), and pmaxGFP (GFP; Amaxa). Primary antibodies and dilutions for Western blotting: anti-acetylated-histone-H3K9 (ab10812; 1:500), anti-acetylated-α-tubulin [6-11B-1] (ab24610; 1:5000), anti-β-actin [mAbcam 8226] (ab8226; 1:2000), anti-Fis1 (ab71498; 1:250), anti-HDAC6 (ab82557; 1:1000), anti-mitofusin2 [NIAR164] (ab124773; 1:1000), anti-succinate dehydrogenase complex subunit A [2E3GC12FB2AE2] (SDHA; ab14715; 1:1000) were from Abcam; anti-α-tubulin [11H10] (#2125; 1:1000), anti-histone-H3 [96C10] (#3638; 1:1000), anti-LC3A/B (#4108; 1:1000) and anti-SQSTM1/p62 (#5114; 1:500) were from Cell Signaling; anti-OPA1 (612606; 1:1000) was from BD Biosciences; anti-acetylated-cortactin (09-881, 1:400) was from Merck-Millipore.

2.2. Drugs and reagents

The HDAC6 inhibitor tubastatin A (TBA) (Selleck Chemicals) was dissolved in dimethyl sulfoxide (DMSO), present at 0.1% in all treatment and control conditions ('solvent'). With the proviso that studies in cells typically require higher concentrations, studies in isolated HDAC isoforms suggest that TBA is HDAC6 selective — isolated enzyme IC_{50} values are 15 nM for HDAC6 and over 1000-fold higher for other HDAC isoforms, except for HDAC8 which is 60-fold higher [23]. Here we use TBA always at 1 μM, as previously described for neurons [24,25]. TBA treatment efficacy is shown in Supplementary Figs. 1 and 2E. Fura-2 AM, MitoTracker Green FM and cell culture reagents were from Invitrogen. All other reagents were from Sigma-Aldrich, unless otherwise stated.

2.3. Neuronal culture and transfection

Sister cortical and striatal primary cultures were generated from Wistar rat embryos as previously described [7,26], in full compliance with European Union directive 2010/63/EU. Cortical and striatal cells were plated at 10^3 cells per mm^2 on polyethylenimine coated glass coverslips and maintained in culture medium (Neurobasal supplemented with 2% B27, 1% fetal bovine serum, 1% penicillin/streptomycin and 1% GlutaMAX) at 37 °C, 5% CO_2. Cytosine arabinoside (10 μM) was added 48 h after plating to prevent glial proliferation. For neuronal transfection, culture medium was replaced with a mixture of 450 μl Neurobasal (with 1% Glutamax) and 50 μl Opti-MEM (containing 0.3–0.5 μg DNA, 0.5 μl Lipofectamine LTX and 0.5 μl Plus Reagent; Invitrogen). Following 30–45 min incubation (37 °C, 5% CO_2) neurons were washed twice with Dulbecco's modified Eagle medium prior to restoring the conditioned culture medium. The average transfection efficiency was 5%, allowing single neuron identification for analyzing neurites, mitochondria, LC3-vesicles, or mHtt levels, without excessive overlap between cells.

2.4. Neurite morphology, mitochondrial occupancy, size and number

Neurons with 10 days *in vitro* (DIV) were fixed (4% paraformaldehyde, 37 °C for 15 min) after 24 h transfection with GFP and mtDsRed, and imaged with an inverted Eclipse TE300 microscope system (Nikon; 60× PlanFluor 0.85 NA air objective; Polychrome II monochromator, TILL Photonics; C6790 CCD camera and Aquacosmos 2.5 software, Hamamatsu). Sholl analysis ([27]; ImageJ) with 1 μm-spaced concentric circles was performed on binary images (following background correction and thresholding), to calculate neurite branching peaks (intersection maxima), outgrowth (summed intersections), and mitochondrial fractional occupancy (mitochondrial intersections divided by neuritic intersections). Particle analysis (ImageJ) was used to calculate mitochondrial number and size (Feret diameter) in neurons divided into 'mitochondrial regions', each comprising the area between two circles of increasing radii: α-region (15–30 μm); β-region (30–80 μm); γ-region (80–130 μm).

2.5. Mitochondrial motility

Neurons at 10 DIV were loaded with Fura-2 AM (4 μM; for labeling neurites; 380 nm excitation) and MitoTracker Green (50 nM; for labeling mitochondria; 488 nm excitation [28]) for 30 min, washed twice and live imaged (5 s intervals for 10 min) in recording media (133 mM NaCl, 5 mM KCl, 1.3 mM $CaCl_2$, 1 mM $MgCl_2$, 1 mM Na_2SO_4, 0.4 mM KH_2PO_4, 15 mM glucose, 20 mM HEPES, pH 7.4) at 37 °C. The proportion of motile mitochondria was assessed *via* kymographs (20 representative lines per video; Multi Kymograph — J. Rietdorf and A. Seitz).

2.6. Mitochondrial DNA (mtDNA) levels

Total DNA was extracted with DNeasy Blood & Tissue Kit (Qiagen) and qPCR was performed with iQ5 System (Bio-Rad) using iQ SYBR Green Supermix (Bio-Rad). Primers for mtDNA (MTND1 gene): forward 5′-AATACGCCGCAGGACCATTC, reverse 5′-GGGGTAGGATGCTCGGATTC. Primers for nuclear DNA (nDNA; eEF1A gene): forward 5′-AGCCAAGT GCTAATGTAAGTGAC, reverse 5′-CCCTTGAACCACGGCATCTA. Relative quantifications were performed with the Pfaffl method (correcting for measured efficiencies) [29].

2.7. Western blotting

Neurons were rinsed with ice-cold phosphate-buffered saline (PBS), lysed in buffer containing 150 mM NaCl, 0.5% deoxycholate, 0.1% SDS, 1% Triton X-100, 50 mM Tris (pH 8.0), and protease inhibitors. Protein was quantified by Bradford assay (Bio-Rad). Samples were boiled in Laemmli buffer, loaded at 20–25 μg per lane in polyacrylamide gels, electrophoresed under reducing conditions, and electroblotted to polyvinylidene difluoride membranes (PVDF; Millipore). Membranes were blocked in PBS with 0.05% Tween 20 (PBST) containing 5% non-fat dry milk, then incubated overnight at 4 °C with primary antibodies (diluted in PBST with 5% BSA — bovine serum albumin), followed by washing in PBST and incubation with respective horseradish peroxidase conjugated antibodies for detection by enhanced chemiluminescence.

2.8. Immunofluorescence

Neurons were fixed with 4% paraformaldehyde for 15 min at 37 °C, washed 3 times in PBS, permeabilized and blocked with 0.1% Triton X-100 and 3% BSA in PBS (Abdil) for 30 min. Neurons were then incubated for 1 h with primary antibody (anti-acetylated-cortactin, 1:150 in Abdil), and washed 3 times with 0.1% Triton X-100 in PBS, followed by

1 h incubation with Alexa Fluor 488 conjugated secondary antibody (Invitrogen; A-11034; 1:200 in Abdil). After assembly in fluorescent mounting medium (Dako), neurons were imaged with the aforementioned Eclipse TE300 system, ensuring non-saturating identical equipment settings for intensity comparisons between treatments.

2.9. LC3-vesicle dynamics

Neurons expressing mCherry-EGFP-LC3B were live imaged at 8–10 DIV (48 h post-transfection) in culture media at 37 °C, 5% CO_2, using an Axiovert 200 M, with LSM510 and a 63× Plan-Apochromat 1.4 NA oil objective (Zeiss). Combining acid-sensitive EGFP (488 nm excitation) with acid-insensitive mCherry (543 nm excitation) allows distinction of autophagosomes (EGFP + mCherry signal) from autolysosomes (mCherry signal only) [30]. LC3-positive vesicles were counted in whole somata Z-stacks. Cytoplasmic volume was measured with 3D Objects Counter (F. Cordelières), deleting nuclei and using diffuse EGFP-LC3 fluorescence to define somatic boundaries. Vesicle motility parameters were analyzed with MTrackJ in 10 min videos at 3 s intervals, acquiring on the mCherry channel only (minimum velocity threshold was 0.1 μm/s; [31]). Vesicles crossing the first axonal branch towards the soma were expressed as events per 5 min (retrograde flux).

2.10. Huntingtin proteostasis

Neurons were transfected either with 'wild-type' Htt (wtHtt; Q23) or mHtt (Q74) encoding plasmids at 5 DIV [20], and live imaged at 24 and 48 h post-transfection in culture medium at 37 °C, 5% CO_2. Fluorescently tagged wtHtt exon 1 (EGFP-Htt^{ex1}Q23) and mHtt exon 1 (EGFP-Htt^{ex1}Q74) were excited at 488 nm and imaged with an inverted fluorescence microscope equipped with a 20× air objective, ensuring non-saturating identical equipment settings for fluorescence intensity comparisons. After imaging at 24 h post-transfection (6 DIV), neurons were treated with either solvent or TBA and re-imaged 24 h later (7 DIV; 48 h post-transfection). Transfected neurons were screened for the presence of aggregates and their location (soma and neurites), and their counts expressed in percentage of EGFP-positive neurons. Diffuse levels of wtHtt or mHtt were measured by the average somatic EGFP fluorescence in neurons without visible aggregates.

2.11. Image processing and data analysis

Image processing was performed with ImageJ (http://rsbweb.nih.gov/ij/; National Institutes of Health) using the indicated plugins. Numerical data calculations were automated in Excel spreadsheets (Microsoft). Other data analyses and statistical calculations were performed using Prism 6.0 (GraphPad Software). Two-tailed Student's *t* test was used when comparing two groups, one-way ANOVAs with Dunnet's post-hoc when comparing three or more groups, and two-way ANOVA with Sidák's post-hoc when testing the interaction plus the main effects of region (cortical × striatal) and treatment (solvent × drugs). Curve fit comparisons in nonlinear regression analyses were performed with extra sum-of-squares *F* test. Unless otherwise stated, data are mean ± SEM of the *n* specified in figure legends.

3. Results

3.1. Mitochondria in striatal neurons are less motile and more balanced towards fission than mitochondria in cortical neurons

Neurons are highly polarized post-mitotic cells that distribute their mitochondria throughout neurites [32]. To investigate whether mitochondrial dynamics differ between striatal and cortical neurons, we started by comparing neurite morphology and relative mitochondrial levels in 10 DIV cultures. Cortical neurons were more branched than striatal neurons, but the average neurite outgrowth of the two populations was similar (Fig. 1A,B — white bars). The proportion of neurite length occupied by mitochondria was not significantly different in striatal and cortical neurons (Fig. 1Ci). Together with similar mtDNA/nDNA ratios (Fig. 1D), these results show that under our experimental conditions cortical and striatal neurons present identical mitochondrial levels.

To compare the mitochondrial fission–fusion balance, we measured mitochondrial size and number in three concentric 'mitochondrial regions' progressively away from soma (α-, β-, and γ-regions; Fig. 2A), and found that mitochondrial size was significantly affected by distance from soma, decreasing from the α- towards the γ-region (Fig. 2B). We also detected that mitochondria in striatal neurons were significantly smaller, but more numerous than in cortical neurons (Fig. 2B,C – white bars). These data, together with identical mitochondrial levels (Fig. 1C,D) and higher expression of the fission-associated Fis1 protein in striatal neurons (Fis1/SDHA, Table 1; Supplementary Fig. 2), indicate that the striatal mitochondrial population is intrinsically more balanced towards fission. Moreover, when we compared mitochondrial motility, we found that mitochondria were less motile in striatal than cortical neurons (Fig. 2D), and that this correlated with decreased α-tubulin acetylation in the striatal population (Fig. 2E). Significantly, we detected higher expression of the α-tubulin deacetylase HDAC6 in striatal neurons (Fig. 2F), which could explain why striatal neurons present lower α-tubulin acetylation, and account for their reduced mitochondrial motility. Indeed, α-tubulin acetylation has been directly correlated with recruitment of motor proteins, thereby promoting microtubule-mediated transport [12,33]. Given that increasing mitochondrial motility likely increases mitochondria contact and fusion-probability, we next tested whether increasing α-tubulin acetylation by HDAC6 inhibition could modulate the mitochondrial fission–fusion balance in neurons.

3.2. HDAC6 inhibition increases mitochondrial motility and promotes mitochondrial fusion in striatal neurons

To assess the effects of HDAC6 inhibition on mitochondrial dynamics, we treated neurons with 1 μM TBA (treatment efficacy and selectivity was confirmed by detecting increased acetylation of the HDAC6-substrate α-tubulin-K40, without off-target increases in histone-H3K9; Fig. 2E; Supplementary Fig. 1). Treatment with TBA significantly increased the proportion of motile mitochondria in cortical and striatal neurons (Fig. 2D), without modifying mitochondrial levels (Fig. 1C,D) or the expression of fission–fusion proteins (Table 1; Supplementary Fig. 2). In cortical neurons, TBA had no significant effect on mitochondrial size and number (Fig. 2B,C). In striatal neurons, however, TBA increased the size and reduced the number of mitochondria (Fig. 2B,C). These results indicate that by increasing the low mitochondrial motility of striatal neurons, TBA treatment promotes mitochondrial contact and fusion, thereby modulating their fission–fusion balance.

Previous studies with HDAC6-deficient cell lines implicated HDAC6 in mitochondrial clearance [16] and in autophagosome–lysosome fusion [14]. However, our present findings show that pharmacological HDAC6 inhibition with TBA increases α-tubulin acetylation without altering mitochondrial levels (Fig. 1C,D), suggesting unaltered mitochondrial clearance in neurons. Moreover, HDAC6-knockout mice show no significant neuropathology [17,18], which challenges the role of HDAC6 in neuronal autophagosome–lysosome fusion, a crucial process for neuronal homeostasis [19]. Therefore, we next investigated how pharmacological HDAC6 inhibition with TBA impacts autophagosome–lysosome fusion in live neurons.

3.3. HDAC6 inhibition does not block neuronal autophagosome–lysosome fusion, but instead increases autophagic flux

To investigate the effects of HDAC6 inhibition on neuronal autophagosome–lysosome fusion, we imaged live neurons expressing

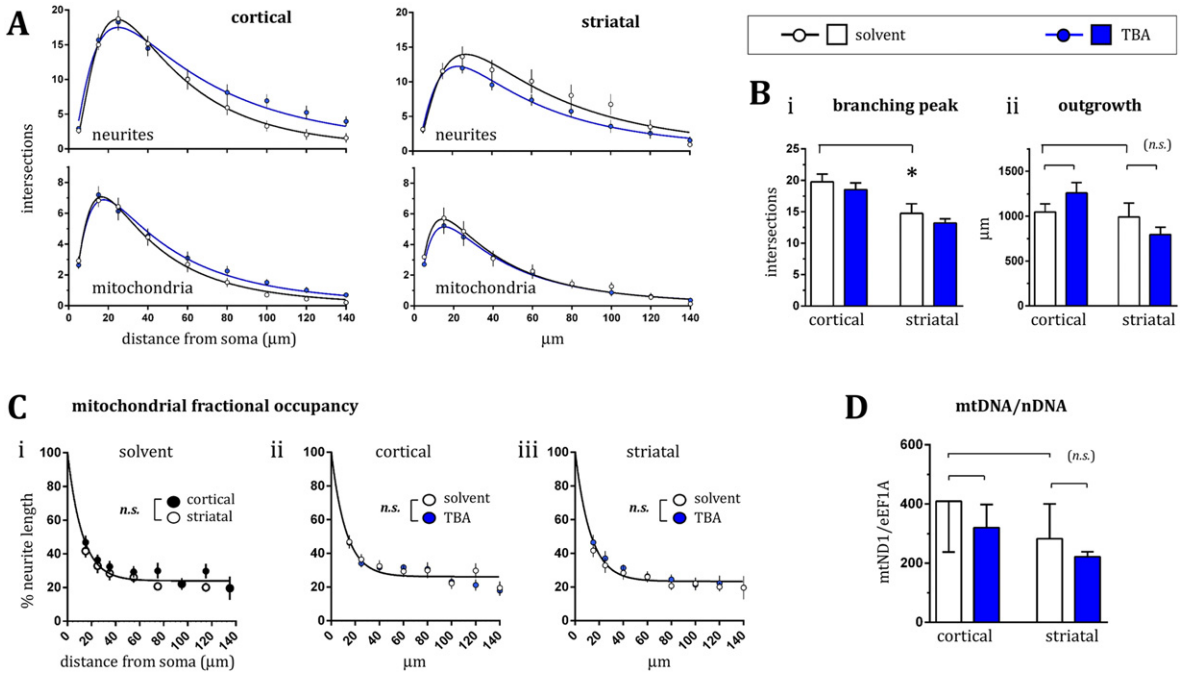

Fig. 1. Mitochondrial fractional occupancy and mtDNA levels in cortical and striatal neurons. (A–D). Cortical and striatal neurons following treatment with solvent or 1 μM TBA for 72 h. (A) Intersections with neurites (top) or mitochondria (bottom) as a function of distance from soma (Sholl analysis with log-normal curve fits); (B) (i) Neurite branching peak and (ii) outgrowth; (C) mitochondrial fractional occupancy with distance from soma (one-phase decay curve fit); $n = 11–17$ neurons from 3 independent cultures, per treatment condition. (D) Mitochondrial DNA levels relative to nuclear DNA; $n = 3$ independent cultures. *n.s.*, not significant ($p > 0.05$); $^{*}p < 0.05$, to solvent-treated cortical neurons; $^{\#}p < 0.05$ to solvent-treated striatal neurons.

mCherry-EGFP-LC3. Under control conditions (solvent), the vast majority of somatodendritic LC3-vesicles were autolysosomes (acidified, with loss of EGFP-fluorescence; Fig. 3Ai), indicating that constitutive autophagosome–lysosome fusion is highly efficient in neurons [34]. Inhibition of the lysosomal proton pump with bafilomycin A1 (BAF) impaired LC3-vesicle acidification (EGFP fluorescence retained; Fig. 3Aiii)

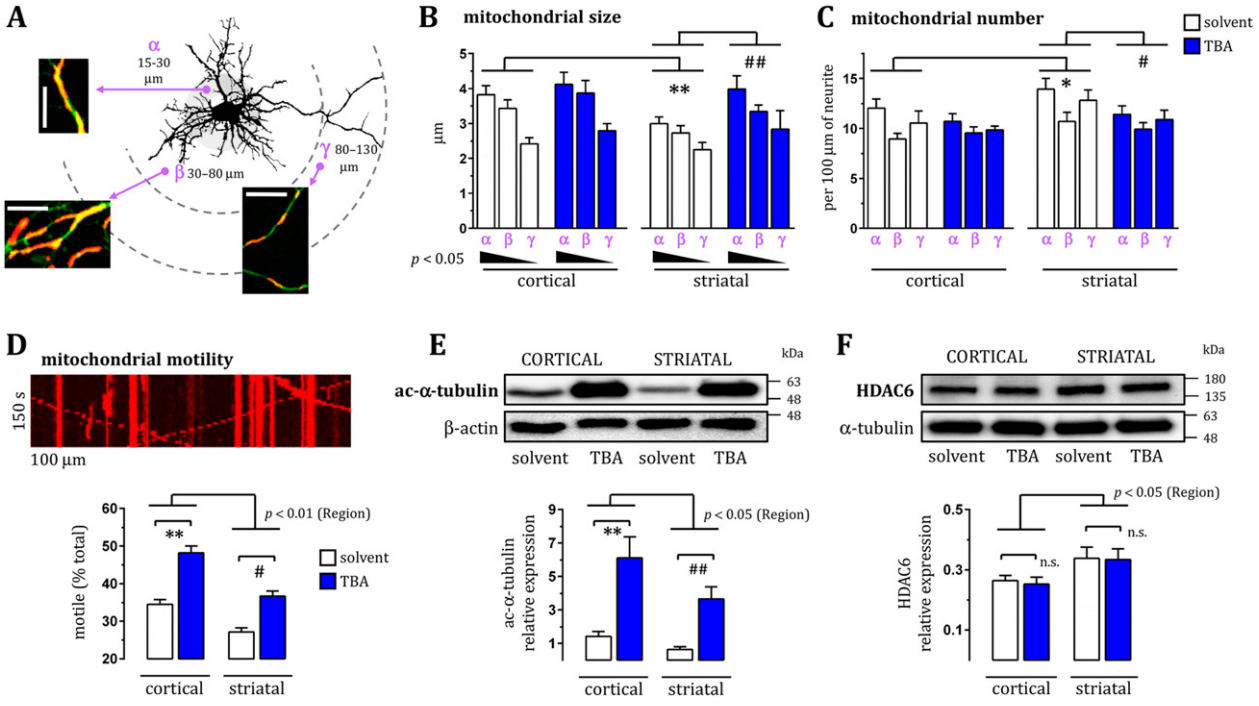

Fig. 2. Mitochondrial dynamics and HDAC6 levels in cortical and striatal neurons. (A) Representative neuron divided in encircled 'mitochondrial regions' α, β, γ, and respective radii. Insets show mitochondria (mtDsRed) and neurites (GFP) with 10 μm scale bars. (B, C) Mitochondrial size and number quantification within the α, β, and γ regions of neurons treated with solvent or 1 μM TBA for 72 h. Black triangles denote significant effects of region (α towards γ) on mitochondrial size ($p < 0.05$, ANOVA linear trend); $n = 15–21$ neurons from 3 independent cultures, per treatment condition. (D) Mitochondrial motility and representative kymograph; $n = 3–10$ independent cultures (296–417 individual mitochondria analyzed per treatment condition in each culture). (E, F) Representative immunoblots and quantification of acetylated α-tubulin levels (E) and of HDAC6 levels (F) in neurons treated with solvent or 1 μM TBA for 24 h; $n = 4$ independent cultures. Region *p* values are from two-way ANOVAS; *n.s.*, not significant ($p > 0.05$); $^{*}p < 0.05$, $^{**}p < 0.01$, to solvent-treated cortical neurons; $^{\#}p < 0.05$, $^{\#\#}p < 0.01$ to solvent-treated striatal neurons.

Table 1
Mitochondrial fission-fusion indicators.

	Striatal/cortical	Cortical	Striatal
	Solvent/solvent	TBA/solvent	TBA/solvent
Fis1/SDHA	↑ 1.35 ± 0.07, $p < 0.01$	0.85 ± 0.11, $p = 0.23$	0.91 ± 0.13, $p = 0.46$
OPA1/SDHA	1.11 ± 0.04, $p = 0.07$	0.97 ± 0.08, $p = 0.66$	0.96 ± 0.17, $p = 0.64$
Mfn2/SDHA	1.11 ± 0.07, $p = 0.20$	1.03 ± 0.11, $p = 0.87$	1.05 ± 0.07, $p = 0.48$

Quantification of protein levels by immunoblot densitometry. Data are mean ± SEM of the ratios to solvent; $n = 3$–7 independent cultures; $p < 0.05$, ratio paired t test. Arrows indicate direction of differences.

and lysosomal digestion (p62 accumulation; BAF: Fig. 3B, Table 2), as predicted for impaired autophagosome–lysosome fusion [34]. Treatment with TBA increased α-tubulin acetylation (Fig. 2E) without impairing LC3-vesicle acidification (Fig. 3Aiv,v) or p62 digestion (Fig. 3B, Table 2). These results show that TBA inhibits HDAC6-mediated α-tubulin deacetylation without blocking neuronal autophagosome–lysosome fusion.

Cortactin deacetylation by HDAC6 was found necessary for constitutive autophagosome–lysosome fusion in fibroblasts. We therefore tested if TBA modified cortactin acetylation in neurons. Under control conditions, *in situ* acetyl-cortactin immunoreactivity was primarily detected in proximal neurites (Fig. 3C), with some cortical and striatal neurons showing nuclear immunoreactivity, as previously reported for hippocampal neurons [35]. Treatment with TBA increased neuronal acetyl-cortactin immunoreactivity *in situ* (Fig. 3C), although this was not confirmed by immunoblotting (Fig. 3D). The function of acetyl-cortactin in neurons is mostly unknown [35]; however, given that cortactin is scarce throughout the axons [36,37] – where most autophagosome-fusion events occur [38,39] – cortactin may not be critical for such events in neurons.

To investigate whether HDAC6 inhibition and the resulting increase in α-tubulin acetylation modified the dynamics of neuronal LC3-vesicles, we monitored the direction and velocity of LC3-vesicles in distal axons (>400 μm from soma), the retrograde LC3-vesicle flux through the first axonal branch (a critical converging point for vesicles moving towards the soma), and we also quantified somatic autolysosomes (Fig. 4). Under control conditions, most LC3-vesicles in distal axons were autophagosomes (mCherry- and EGFP-positive; Fig. 4A) and exhibited robust retrograde movement (Fig. 4B,C), as previously described [31,38]. Treatment with TBA modified neither LC3-vesicle direction (Fig. 4C) nor velocity (Fig. 4C,D), but significantly increased the retrograde flux through the first axonal branch (Fig. 4E,F), and the number of somatic autolysosomes (Fig. 4G,H), suggesting that more autophagosomes are being formed and converted into autolysosomes while moving towards the soma. TBA treatment also increased LC3-II expression, while decreasing p62 levels (Fig. 3B, Table 2), as predicted for increased formation of autophagosomes together with enhanced lysosomal digestion [34], indicating that TBA increases autophagic flux. Given the evidence that huntingtin proteostasis is regulated by autophagy [20], we therefore investigated whether TBA treatment could modulate huntingtin proteostasis in cortical and striatal neurons.

3.4. The HDAC6 inhibitor TBA promotes clearance of diffuse mHtt in striatal neurons

We compared huntingtin proteostasis in cortical and striatal neurons expressing either an EGFP-wtHtt construct with 23Q ('wild-type') or an EGFP-mHtt construct with 74Q ('mutant'), which were imaged at 24 h and 48 h post-transfection (Fig. 5A). Neurons expressing wtHtt presented a diffuse pattern of EGFP distribution (Fig. 6A), with no visible aggregates at any imaging timepoint (Fig. 5A). In contrast, neurons expressing mHtt presented more diverse EGFP distribution

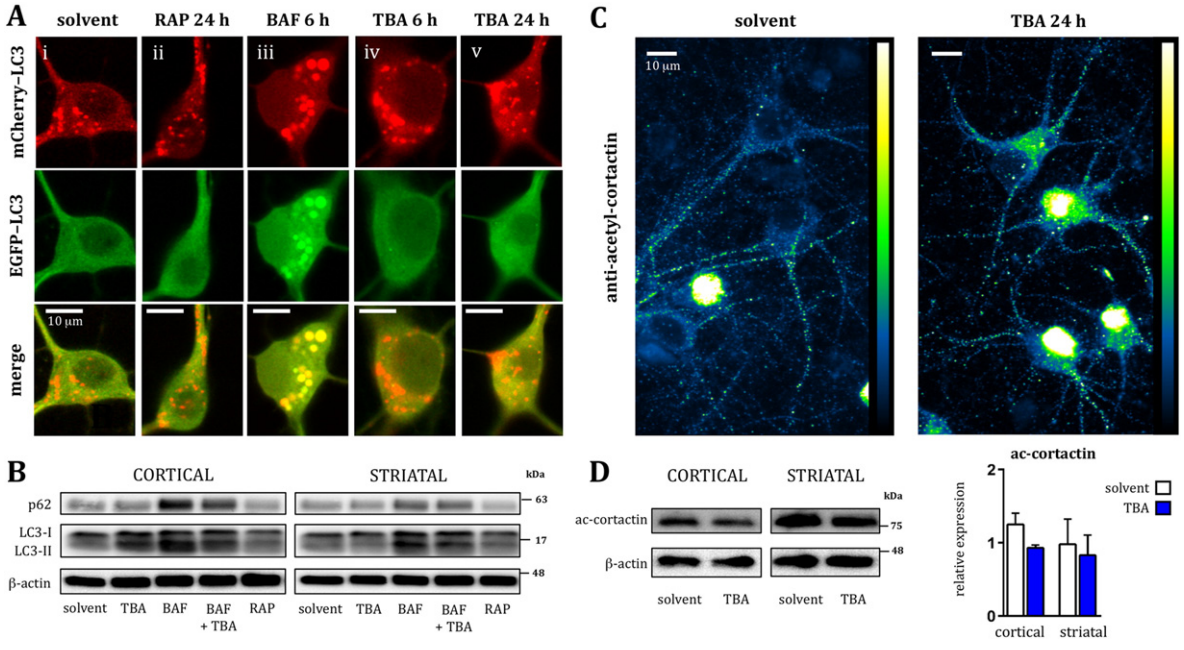

Fig. 3. Neuronal autophagosome-lysosome fusion and autophagy markers. (A) Representative somata of cortical neurons expressing mCherry-EGFP-LC3, imaged live following the indicated treatments: RAP — 10 nM rapamycin, BAF — 25 nM bafilomycin A1, TBA — 1 μM tubastatin A. (B) Immunoblot for autophagy markers: neurons were incubated with solvent, TBA or RAP for 24 h before protein extraction; BAF was present only for the last 6 h of incubation (see Table 2 for quantifications). (C) Representative immunofluorescence images of acetyl-cortactin in cortical neurons treated with solvent or TBA for 24 h. (D) Immunoblot for acetyl-cortactin with respective quantification relative to β-actin; $n = 4$ independent cultures.

Table 2
Autophagy markers in cortical and striatal neurons.

	LC3-II/β-actin		p62/β-actin	
	Cortical	Striatal	Cortical	Striatal
TBA/solvent	↑ 1.48 ± 0.10, $p < 0.05$	↑ 1.25 ± 0.04, $p < 0.01$	0.88 ± 0.20, $p = 0.52$	↓ 0.82 ± 0.02, $p < 0.05$
BAF/solvent	↑ 1.79 ± 0.12, $p < 0.05$	↑ 2.43 ± 0.21, $p < 0.01$	↑ 1.90 ± 0.18, $p < 0.05$	1.22 ± 0.17, $p = 0.34$
RAP/solvent	1.18 ± 0.11, $p = 0.24$	↑ 1.72 ± 0.17, $p < 0.05$	0.66 ± 0.13, $p = 0.14$	↓ 0.58 ± 0.08, $p < 0.05$

Quantification of protein levels by immunoblot densitometry. Data are mean ± SEM of the ratios to solvent; $n = 3$–4 independent cultures; $p < 0.05$, ratio paired t test. Arrows indicate direction of differences.

patterns: some neurons presented diffuse EGFP only (Fig. 5B — neuron 1; Fig. 6Bi), while others presented somatic (Fig. 5B — neuron 2) and/or neuritic aggregates (Fig. 5B — neuron 3 and box 3′).

The overall proportion of neurons with mHtt aggregates at 24 h was higher for cortical than for striatal neurons, increasing at identical rates for both populations towards 48 h (Fig. 5Ci). Within mHtt aggregate-containing neurons, the proportion with neuritic aggregates at 24 h was similar and increased over time without significant differences between cortical and striatal neurons (Fig. 5Di). In neurons without aggregates, diffuse mHtt levels were higher at 24 h and decreased over time for cortical neurons, whereas the opposite pattern was observed for striatal neurons where diffuse mHtt continued to increase towards 48 h (Fig. 6Bii). In contrast, diffuse wtHtt levels showed no significant changes over time within cortical or striatal neurons (Fig. 6Aii), thus highlighting that the differential proteostasis of diffuse huntingtin is polyQ-dependent. Moreover, these results suggest that the time-dependent clearance of diffuse mHtt is more efficient in cortical than striatal neurons (Fig. 6Bii). Given the aforementioned data indicating that HDAC6 inhibition increases neuronal autophagic flux, we investigated whether TBA treatment modulated huntingtin proteostasis in neurons.

Treatment with the HDAC6 inhibitor TBA did not modify the overall proportion of cortical or striatal neurons with mHtt aggregates (Fig. 5Cii), while showing a trend for reducing mHtt aggregates in striatal neurites (Fig. 5Dii). Moreover, treatment with TBA significantly reduced diffuse mHtt levels in striatal neurons (Fig. 6Biii), but did not alter those of wtHtt (Fig. 6Aiii). Thus, pharmacological HDAC6 inhibition in neurons seems to increase the clearance of diffuse huntingtin in a polyQ-dependent manner.

4. Discussion

Here we have shown that wild-type striatal and cortical neurons present intrinsic differences in mitochondrial fission–fusion and trafficking dynamics. Mitochondria in striatal neurons are more balanced towards fission and are less motile than those in cortical neurons.

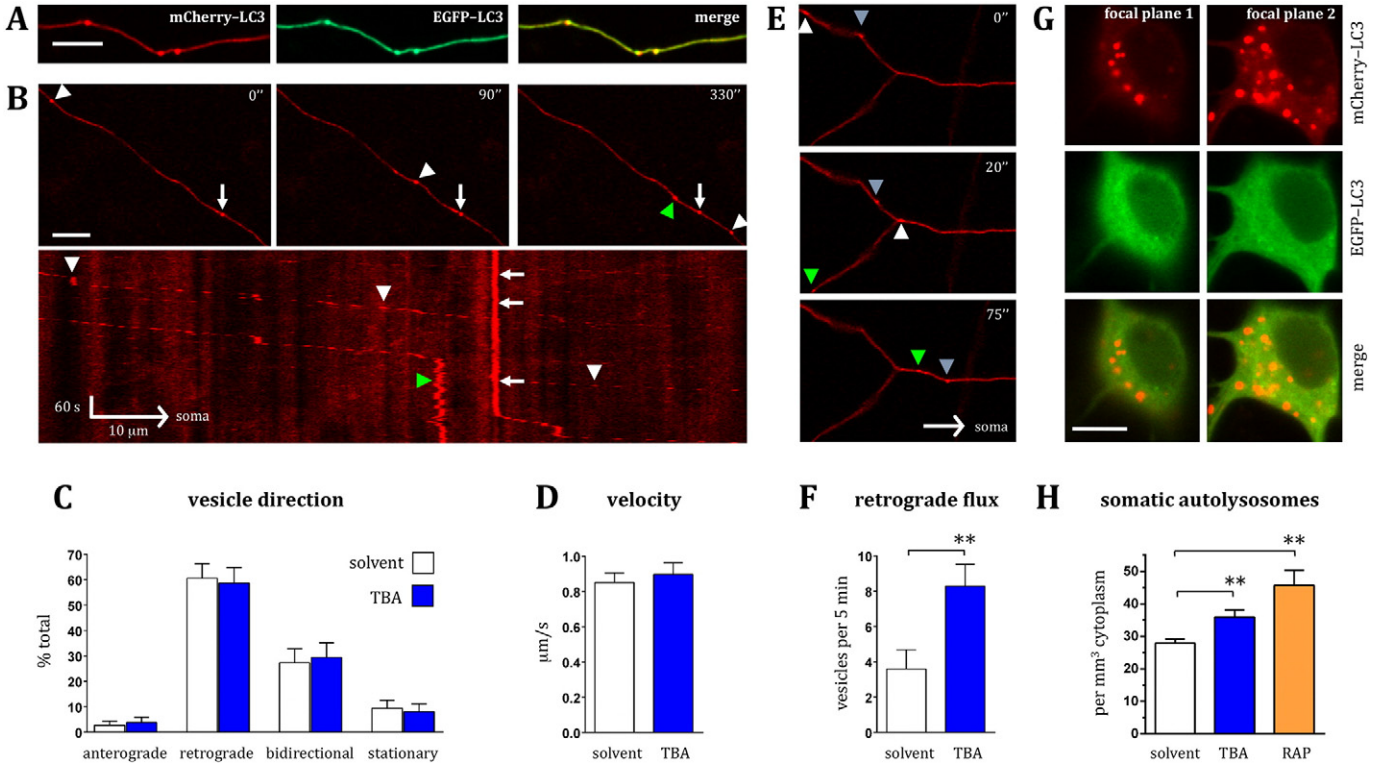

Fig. 4. Neuronal LC3-vesicle dynamics. (A) mCherry- and EGFP- positive LC3-vesicles in distal axons of live cortical neurons. (B) Time-lapse (top) and kymograph (bottom) showing stationary (arrow) and moving (arrowhead) LC3-vesicles in a distal axon (only the mCherry channel is shown). (C) Movement direction of LC3-vesicles in distal axons of cortical neurons treated with solvent or TBA (1 μM, 24 h); $n = 21$–26 axonal sections from 20–21 neurons from 4 independent cultures. (D) Retrograde LC3-vesicle velocity in distal axons of cortical neurons treated with solvent or TBA; $n = 92$–109 vesicles from 19–20 neurons from 4 independent cultures. (E) LC3-vesicles (arrowheads) moving through the first axonal branch towards the soma. (F) Retrograde flux of LC3-vesicles through the first axonal branch of cortical neurons treated with solvent or TBA; $n = 11$–14 neurons from 2 independent cultures. (G) Cortical soma showing different number of LC3-vesicles depending on the focal plane (left *vs.* right). (H) Quantification of autolysosomes (mCherry signal only) in cortical neuronal somata Z-stacks imaged after 24 h treatment with solvent, TBA or rapamycin (RAP, 10 nM); $n = 13$–68 neurons from 2–7 independent cultures. $^{**}p < 0.01$ *vs.* solvent. Scale bars: 10 μM.

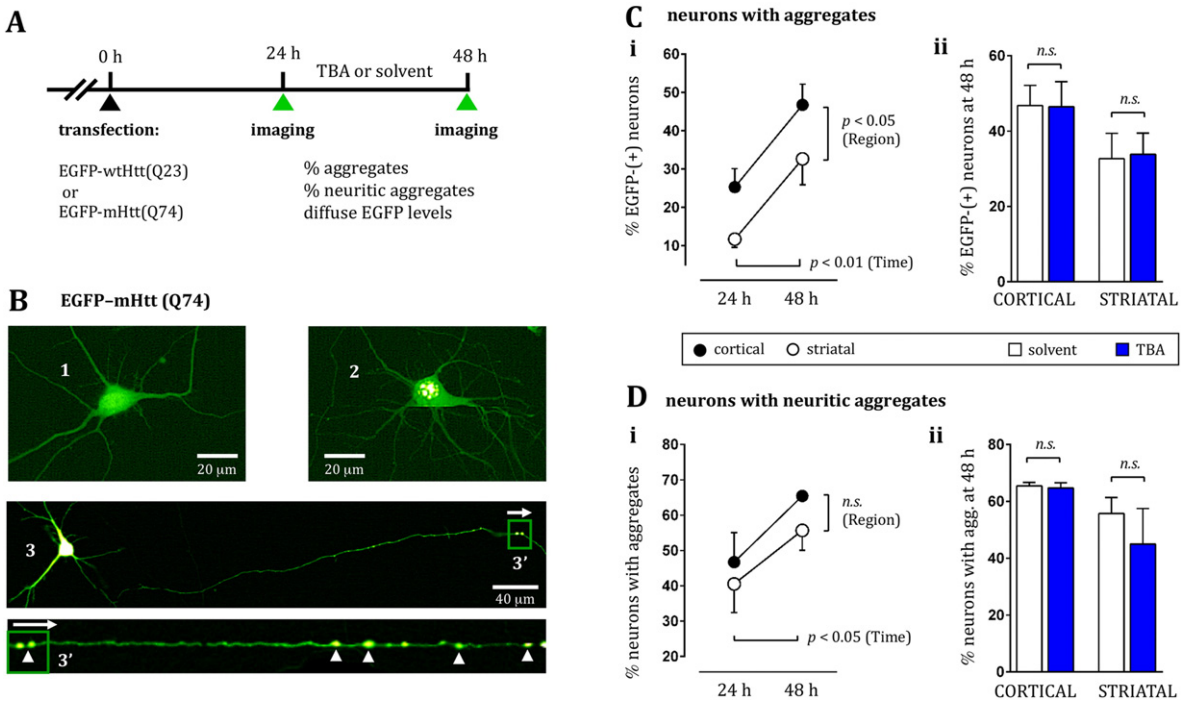

Fig. 5. Huntingtin proteostasis in cortical and striatal neurons. (A) Schematic experimental design for assessing wtHtt and mHtt proteostasis in cortical and striatal neurons and its modulation by HDAC6 inhibition. (B) Representative mHtt (EGFP-Htt^{ex1}Q74) expression patterns: (1) diffuse; (2) somatic and (3, 3′) neuritic aggregates. (3′) straightened axonal section to the right of green box. (C and D) (i) region × time: comparison of solvent-treated cortical and striatal neurons from 24 to 48 h; (ii) region × treatment: comparison of cortical and striatal neurons at 48 h, following 24 h treatment with solvent or 1 μM TBA. (C) Neurons with mHtt aggregates in percentage of EGFP-positive neurons; (D) Neurons with neuritic aggregates, in percentage of aggregate-containing neurons; $n = 3$ independent cultures with 599–852 EGFP-positive neurons per experimental group. Region and time p values are from two-way ANOVAS.

The HDAC6 inhibitor TBA altered the mitochondrial fission–fusion balance by increasing mitochondrial motility and promoting fusion. Pharmacological HDAC6 inhibition with TBA did not block neuronal autophagosome-lysosome fusion, but increased autophagic flux and reduced diffuse mHtt in striatal neurons, without changing the levels of wtHtt. These data provide insight into HD striatal vulnerability and experimental therapeutics with HDAC6 inhibition, as addressed below.

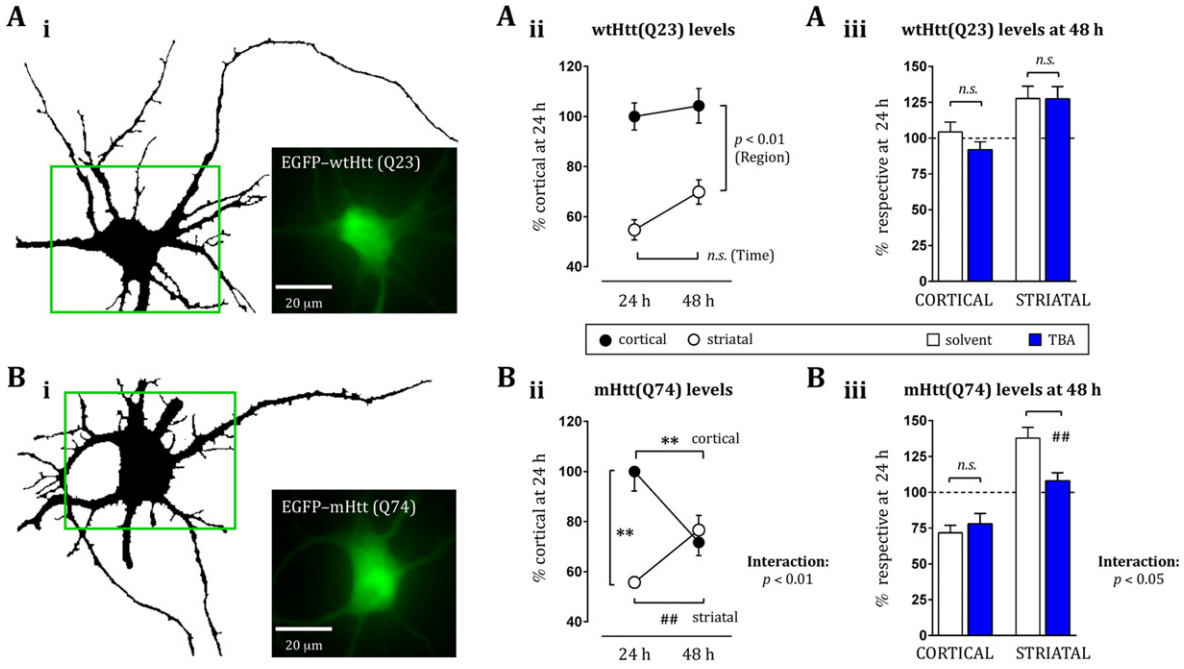

Fig. 6. Levels of diffuse wild-type and mutant huntingtin in cortical and striatal neurons. Data are from neurons expressing only diffuse huntingtin (wtHtt or mHtt) at 24 or 48 h. (A, B) (i) Representative neurons expressing diffuse wtHtt (EGFP-Htt^{ex1}Q23) or mHtt (EGFP-Htt^{ex1}Q74); (ii) Region × time: comparison of solvent-treated cortical and striatal neurons from 24 to 48 h; (iii) Region × treatment: comparison of cortical and striatal neurons at 48 h, following 24 h treatment with solvent or 1 μM TBA; (Aii, iii) $n = 133$–166 neurons expressing diffuse wtHtt per experimental group, from 2 independent cultures; (Bii, iii) $n = 86$–220 neurons expressing diffuse mHtt per experimental group, from 3–4 independent cultures. Interaction, region, and time p values are from two-way ANOVAS; $^{**}p < 0.01$ to solvent-treated cortical neurons; $^{\#\#}p < 0.01$ to solvent-treated striatal neurons.

4.1. HDAC6 inhibition increases mitochondrial motility and attenuates differences in fission–fusion balance between striatal and cortical neurons

Mitochondrial dysfunction, including impaired calcium handling, excessive fission and reduced trafficking, are associated with HD pathophysiology [2–5]. Previous studies have proposed that excessive mitochondrial fragmentation in HD involves the direct interaction between mHtt and the fission-mediator Drp1, upregulating its GTPase activity [40,41]. Importantly, the upregulation of Drp1 GTPase activity was found stronger in the striatum than in the cortex of BACHD mice [41]. Here we show that mitochondria in wild-type striatal neurons are intrinsically more balanced towards fission and present higher expression levels of the Drp1 receptor Fis1 than cortical neurons. Higher Fis1 levels may increase the susceptibility of striatal neurons to the upregulation of Drp1 activity by mHtt and contribute towards striatal neurons being precociously affected in HD. Additionally, we show that mitochondria in striatal neurons display lower motility than in cortical neurons. Such intrinsically lower motility may contribute to the more striking inhibition of mitochondrial trafficking by diffuse mHtt in striatal [42] than in cortical neurons [43]. Mechanistically, the higher HDAC6 expression that we found in striatal than in cortical neurons plausibly explains the lower α-tubulin acetylation levels and also the reduced motility of striatal mitochondria.

TBA, the inhibitor of HDAC6, increased tubulin acetylation and mitochondrial motility in cortical and striatal neurons, consistent with increased motor affinity to acetylated microtubules [12,33], and with previous studies in hippocampal [44] or dorsal-root-ganglion neurons [24]. We also show that TBA shifts the mitochondrial fission–fusion balance of striatal neurons towards more fusion, possibly because increasing microtubule-dependent movement increases fusion probability [45,46], particularly when mitochondrial contact probability is otherwise reduced by low motility. Inhibition of mitochondrial fission is emerging as a pharmacological strategy to counteract excessive mitochondrial fission in neurodegenerative diseases, such as HD [47,48]. However, sufficient fission must remain for suitable mitochondrial distribution and quality-control [49–51]. Since TBA treatment promoted mitochondrial fusion in striatal neurons, pharmacological inhibition of HDAC6 warrants further investigation as a strategy to counteract excessive mitochondrial fission in HD.

4.2. HDAC6 inhibition does not block autophagosome–lysosome fusion in neurons, but instead stimulates neuronal autophagic flux

Studies using HDAC6-deficient cell lines suggest that the clearance of damaged mitochondria and misfolded protein aggregates relies on a common autophagic pathway dependent on HDAC6 [16]. Moreover, HDAC6 was reported necessary for constitutive autophagosome–lysosome fusion [14], a crucial step in autophagy. Importantly, the HDAC6 inhibitor TBA was designed to selectively inhibit the deacetylase activity of HDAC6 [23], likely preserving the ubiquitin-binding activity of HDAC6 that is considered important for detecting damaged mitochondria that have been targeted for clearance [16]. Here we show that pharmacological HDAC6 inhibition with TBA effectively increases α-tubulin acetylation in neurons, without blocking their LC3-vesicle acidification and p62 digestion, and without modifying their mtDNA/nDNA levels. Thus, our data suggest that the deacetylase activity of HDAC6 is dispensable for neuronal autophagosome–lysosome fusion, and that the preserved ubiquitin-binding activity in the presence of TBA allows for HDAC6-dependent clearance of ubiquitinated mitochondria.

The present study shows that HDAC6 inhibition induces neuronal autophagic flux. Indeed, the higher LC3-vesicle retrograde flux, more somatic autolysosomes, increased LC3-II and decreased p62 levels we found in TBA-treated neurons, are strongly indicative of increased autophagosomal biogenesis and efficient autophagic clearance [39]. In agreement with our findings, HDAC6 inhibition was recently reported to induce autophagic flux in primary cardiomyocytes [52] and to facilitate the autophagic degradation of Aβ and hyperphosphorylated tau [53].

Acetylated microtubules were reported to allow autophagy stimulation upon nutrient deprivation [54] and to be required for the fusion of autophagosomes and lysosomes [55]. Increased α-tubulin acetylation by HDAC6 inhibition may thus facilitate autophagosome–lysosome fusion and autolysosome formation along the axon. But how might HDAC6 inhibition stimulate autophagosomal biogenesis? We hypothesize that the associated increase in microtubule-dependent transport promotes initiating factor arrival to sites of autophagosomal formation. Such factors might include the endoplasmic reticulum subdomains containing DFCP1 (Double-FYVE-Containing-Protein-1; involved in neuronal autophagosomal biogenesis: [39,56]), the c-Jun-N-terminal-protein-Kinase-1 (JNK1; required for autophagosomal biogenesis: [57]), and the JNK1-interacting protein (JIP1; required for autophagosomal exit from distal axons: [58,54]).

4.3. Striatal and cortical neurons differ in mHtt proteostasis, and HDAC6 inhibition promotes diffuse mHtt clearance

Here we found higher initial levels of diffuse mHtt and more pronounced aggregation in cortical than striatal neurons, consistent with higher initial levels predicting aggregate formation [59,60], and with more aggregates in cortex than striatum in HD patients [61]. In the absence of aggregates, our data suggest that diffuse mHtt accumulates over time in striatal but not in cortical neurons, which is consistent with a longer mean lifetime of mHtt in striatal than cortical neurons [20], and with recent data showing preferential accumulation of mHtt in the striatum [62]. The direct correlation of diffuse mHtt levels with the risk of neuronal death suggests that the toxic species reside within the diffuse fraction [59,60] and, therefore, that treatments capable of reducing diffuse mHtt should hold neuroprotective potential.

Our data show that the HDAC6 inhibitor TBA reduced diffuse mHtt in striatal neurons. Significantly, this effect was specific for the expanded polyQ in mHtt (Q74), given that levels of diffuse wtHtt (Q23) remained unchanged with TBA treatment. Moreover, TBA did not alter the proportion of cortical and striatal neurons with mHtt aggregates, suggesting that the deacetylase activity of HDAC6 is dispensable for aggregate formation and clearance in neurons. These present findings in neurons apparently contrast with studies in HDAC6-knockout cell-lines showing reduced clearance of protein aggregates [63] and reduced autophagic degradation of mHtt [15]. Our findings agree, however, with other studies in neurons, where HDAC6 inhibition alleviated abnormal Aβ and tau accumulation [53,64], and with *in vivo* HDAC6-knockout in R6/2 mice showing no increase in mHtt aggregates [65]. Thus, as previously suggested [65], some of the effects of HDAC6 in cell-lines may not apply to neurons.

HDAC6-knockout R6/2 mice showed neither symptomatic improvement, nor changes in mHtt aggregate load [65]. However, studies reporting increased mHtt clearance upon induction of autophagy have most frequently used 68-97Q mHtt [66–70], whereas HDAC6-knockout R6/2 had an unusually high mHtt polyQ–201Q [65]. Moreover, aggregates precede symptom onset in R6/2 [65], and data from neuronal models predict that diminishing diffuse mHtt levels should be more beneficial in the 'pre-aggregate epoch' [60]. Furthermore, although HDAC6-knockout R6/2 mice showed no changes in global levels of soluble mHtt, their cortex showed decreased soluble mHtt (no data on soluble mHtt was reported for their striatum; [65]). Therefore, it would be valuable to start HDAC6 inhibition at the pre-aggregate epoch and test for delayed symptom onset in HD mice with shorter polyQ and slower disease progression.

5. Concluding remarks

The intrinsic balance towards fission and lower motility of striatal mitochondria may contribute towards the greater sensitivity of striatal

neurons to HD-associated mitochondrial fragmentation and impaired trafficking. Here we show that pharmacological HDAC6 inhibition with TBA approximates the mitochondrial fission–fusion balance and mitochondrial motility of striatal neurons to that of the less HD-vulnerable cortical neurons, increases neuronal autophagic flux, and promotes clearance of diffuse mHtt in striatal neurons. Recent *in vivo* studies support HDAC6 inhibition as a neuroprotective strategy in Alzheimer's disease [18,53], Charcot–Marie–Tooth [24], and amyotrophic lateral sclerosis [71]. The present study supports pharmacological HDAC6 inhibition as a strategy with the potential to reduce striatal vulnerability to HD.

Supplementary data to this article can be found online at http://dx.doi.org/10.1016/j.bbadis.2015.08.012.

Competing interests

The authors declare they have no competing interests.

Authors' contributions

PGD performed the majority of experiments, data analysis, and literature search. JP and TS contributed to image acquisition and analysis of mitochondrial dynamics. ALR and BRP contributed to molecular biology experiments. MRD and JMAO contributed to imaging experiments. PGD and JMAO designed the experiments and wrote the manuscript. All authors read and approved the final manuscript.

Transparency document

The Transparency document associated with this article can be found, in the online version.

Acknowledgment

Work in JMAO's lab was supported by the Fundação para a Ciência e a Tecnologia (FCT) strategic award UID/QUI/50006/2013, and by the research grant PTDC/NEU-NMC/0237/2012 (FCT; PI JMAO), co-financed by the European Union (FEDER, QREN, COMPETE) — FCOMP-01-0124-FEDER-029649. Work in MRD's lab was supported by the Wellcome Trust and Medical Research Council strategic award (WT089698/Z/09/Z). PGD acknowledges FCT for his PhD Grant SFRH/BD/72071/2010. BRP acknowledges FCT for her PostDoc Grant SFRH/BPD/102259/2014. The authors acknowledge the anonymous reviewers for their suggestions that helped improve the final version of the manuscript.

References

[1] C.A. Ross, S.J. Tabrizi, Huntington's disease: from molecular pathogenesis to clinical treatment, Lancet Neurol. 10 (2011) 83–98.
[2] J.M. Oliveira, Nature and cause of mitochondrial dysfunction in Huntington's disease: focusing on huntingtin and the striatum, J. Neurochem. 114 (2010) 1–12.
[3] J.M. Oliveira, Mitochondrial bioenergetics and dynamics in Huntington's disease: tripartite synapses and selective striatal degeneration, J. Bioenerg. Biomembr. 42 (2010) 227–234.
[4] V. Costa, L. Scorrano, Shaping the role of mitochondria in the pathogenesis of Huntington's disease, EMBO J. 31 (2012) 1853–1864.
[5] P.H. Reddy, U.P. Shirendeb, Mutant huntingtin, abnormal mitochondrial dynamics, defective axonal transport of mitochondria, and selective synaptic degeneration in Huntington's disease, Biochim. Biophys. Acta 1822 (2012) 101–110.
[6] A.M. Pickrell, H. Fukui, X. Wang, M. Pinto, C.T. Moraes, The striatum is highly susceptible to mitochondrial oxidative phosphorylation dysfunctions, J. Neurosci. 31 (2011) 9895–9904.
[7] J.M. Oliveira, J. Goncalves, In situ mitochondrial Ca2+ buffering differences of intact neurons and astrocytes from cortex and striatum, J. Biol. Chem. 284 (2009) 5010–5020.
[8] K. Itoh, K. Nakamura, M. Iijima, H. Sesaki, Mitochondrial dynamics in neurodegeneration, Trends Cell Biol. 23 (2013) 64–71.
[9] P.H. Reddy, Increased mitochondrial fission and neuronal dysfunction in Huntington's disease: implications for molecular inhibitors of excessive mitochondrial fission, Drug Discov. Today 19 (2014) 951–955.
[10] A. Leitao-Rocha, P. Guedes-Dias, B.R. Pinho, J.M. Oliveira, Trends in mitochondrial therapeutics for neurological disease, Curr. Med. Chem. 22 (2015) 2458–2467.
[11] P. Guedes-Dias, J.M. Oliveira, Lysine deacetylases and mitochondrial dynamics in neurodegeneration, Biochim. Biophys. Acta 1832 (2013) 1345–1359.
[12] J.P. Dompierre, J.D. Godin, B.C. Charrin, F.P. Cordelieres, S.J. King, S. Humbert, F. Saudou, Histone deacetylase 6 inhibition compensates for the transport deficit in Huntington's disease by increasing tubulin acetylation, J. Neurosci. 27 (2007) 3571–3583.
[13] M.V. Hinckelmann, D. Zala, F. Saudou, Releasing the brake: restoring fast axonal transport in neurodegenerative disorders, Trends Cell Biol. 23 (2013) 634–643.
[14] J.Y. Lee, H. Koga, Y. Kawaguchi, W. Tang, E. Wong, Y.S. Gao, U.B. Pandey, S. Kaushik, E. Tresse, J. Lu, J.P. Taylor, A.M. Cuervo, T.P. Yao, HDAC6 controls autophagosome maturation essential for ubiquitin-selective quality-control autophagy, EMBO J. 29 (2010) 969–980.
[15] A. Iwata, B.E. Riley, J.A. Johnston, R.R. Kopito, HDAC6 and microtubules are required for autophagic degradation of aggregated huntingtin, J. Biol. Chem. 280 (2005) 40282–40292.
[16] J.Y. Lee, Y. Nagano, J.P. Taylor, K.L. Lim, T.P. Yao, Disease-causing mutations in parkin impair mitochondrial ubiquitination, aggregation, and HDAC6-dependent mitophagy, J. Cell Biol. 189 (2010) 671–679.
[17] Y. Zhang, S. Kwon, T. Yamaguchi, F. Cubizolles, S. Rousseaux, M. Kneissel, C. Cao, N. Li, H.L. Cheng, K. Chua, D. Lombard, A. Mizeracki, G. Matthias, F.W. Alt, S. Khochbin, P. Matthias, Mice lacking histone deacetylase 6 have hyperacetylated tubulin but are viable and develop normally, Mol. Cell. Biol. 28 (2008) 1688–1701.
[18] N. Govindarajan, P. Rao, S. Burkhardt, F. Sananbenesi, O.M. Schluter, F. Bradke, J. Lu, A. Fischer, Reducing HDAC6 ameliorates cognitive deficits in a mouse model for Alzheimer's disease, EMBO Mol. Med. 5 (2013) 52–63.
[19] R.A. Nixon, The role of autophagy in neurodegenerative disease, Nat. Med. 19 (2013) 983–997.
[20] A.S. Tsvetkov, M. Arrasate, S. Barmada, D.M. Ando, P. Sharma, B.A. Shaby, S. Finkbeiner, Proteostasis of polyglutamine varies among neurons and predicts neurodegeneration, Nat. Chem. Biol. 9 (2013) 586–592.
[21] E.N. N'Diaye, K.K. Kajihara, I. Hsieh, H. Morisaki, J. Debnath, E.J. Brown, PLIC proteins or ubiquilins regulate autophagy-dependent cell survival during nutrient starvation, EMBO Rep. 10 (2009) 173–179.
[22] Y. Narain, A. Wyttenbach, J. Rankin, R.A. Furlong, D.C. Rubinsztein, A molecular investigation of true dominance in Huntington's disease, J. Med. Genet. 36 (1999) 739–746.
[23] K.V. Butler, J. Kalin, C. Brochier, G. Vistoli, B. Langley, A.P. Kozikowski, Rational design and simple chemistry yield a superior, neuroprotective HDAC6 inhibitor, tubastatin A, J. Am. Chem. Soc. 132 (2010) 10842–10846.
[24] C. d'Ydewalle, J. Krishnan, D.M. Chiheb, P. Van Damme, J. Irobi, A.P. Kozikowski, P. Vanden Berghe, V. Timmerman, W. Robberecht, L. Van Den Bosch, HDAC6 inhibitors reverse axonal loss in a mouse model of mutant HSPB1-induced Charcot–Marie–Tooth disease, Nat. Med. 17 (2011) 968–974.
[25] S. Baltan, S.P. Murphy, C.A. Danilov, A. Bachleda, R.S. Morrison, Histone deacetylase inhibitors preserve white matter structure and function during ischemia by conserving ATP and reducing excitotoxicity, J. Neurosci. 31 (2011) 3990–3999.
[26] J.M. Oliveira, S. Chen, S. Almeida, R. Riley, J. Goncalves, C.R. Oliveira, M.R. Hayden, D.G. Nicholls, L.M. Ellerby, A.C. Rego, Mitochondrial-dependent Ca2+ handling in Huntington's disease striatal cells: effect of histone deacetylase inhibitors, J. Neurosci. 26 (2006) 11174–11186.
[27] D.A. Sholl, Dendritic organization in the neurons of the visual and motor cortices of the cat, J. Anat. 87 (1953) 387–406.
[28] J.M. Oliveira, Techniques to investigate neuronal mitochondrial function and its pharmacological modulation, Curr. Drug Targets 12 (2011) 762–773.
[29] M.W. Pfaffl, A new mathematical model for relative quantification in real-time RT-PCR, Nucleic Acids Res. 29 (2001), e45.
[30] S. Pankiv, T.H. Clausen, T. Lamark, A. Brech, J.A. Bruun, H. Outzen, A. Overvatn, G. Bjorkoy, T. Johansen, p62/SQSTM1 binds directly to Atg8/LC3 to facilitate degradation of ubiquitinated protein aggregates by autophagy, J. Biol. Chem. 282 (2007) 24131–24145.
[31] S. Lee, Y. Sato, R.A. Nixon, Lysosomal proteolysis inhibition selectively disrupts axonal transport of degradative organelles and causes an Alzheimer's-like axonal dystrophy, J. Neurosci. 31 (2011) 7817–7830.
[32] G. Ruthel, P.J. Hollenbeck, Response of mitochondrial traffic to axon determination and differential branch growth, J. Neurosci. 23 (2003) 8618–8624.
[33] N.A. Reed, D. Cai, T.L. Blasius, G.T. Jih, E. Meyhofer, J. Gaertig, K.J. Verhey, Microtubule acetylation promotes kinesin-1 binding and transport, Curr. Biol. 16 (2006) 2166–2172.
[34] D.J. Klionsky, et al., Guidelines for the use and interpretation of assays for monitoring autophagy, Autophagy 8 (2012) 445–544.
[35] T. Catarino, L. Ribeiro, S.D. Santos, A.L. Carvalho, Regulation of synapse composition by protein acetylation: the role of acetylated cortactin, J. Cell Sci. 126 (2013) 149–162.
[36] H. Hering, M. Sheng, Activity-dependent redistribution and essential role of cortactin in dendritic spine morphogenesis, J. Neurosci. 23 (2003) 11759–11769.
[37] B. Racz, R.J. Weinberg, The subcellular organization of cortactin in hippocampus, J. Neurosci. 24 (2004) 10310–10317.
[38] S. Maday, K.E. Wallace, E.L. Holzbaur, Autophagosomes initiate distally and mature during transport toward the cell soma in primary neurons, J. Cell Biol. 196 (2012) 407–417.
[39] S. Maday, E.L. Holzbaur, Autophagosome biogenesis in primary neurons follows an ordered and spatially regulated pathway, Dev. Cell 30 (2014) 71–85.
[40] W. Song, J. Chen, A. Petrilli, G. Liot, E. Klinglmayr, Y. Zhou, P. Poquiz, J. Tjong, M.A. Pouladi, M.R. Hayden, E. Masliah, M. Ellisman, I. Rouiller, R. Schwarzenbacher, B. Bossy, G. Perkins, E. Bossy-Wetzel, Mutant huntingtin binds the mitochondrial

fission GTPase dynamin-related protein-1 and increases its enzymatic activity, Nat. Med. 17 (2011) 377–382.
[41] U.P. Shirendeb, M.J. Calkins, M. Manczak, V. Anekonda, B. Dufour, J.L. McBride, P. Mao, P.H. Reddy, Mutant huntingtin's interaction with mitochondrial protein Drp1 impairs mitochondrial biogenesis and causes defective axonal transport and synaptic degeneration in Huntington's disease, Hum. Mol. Genet. 21 (2012) 406–420.
[42] A.L. Orr, S. Li, C.E. Wang, H. Li, J. Wang, J. Rong, X. Xu, P.G. Mastroberardino, J.T. Greenamyre, X.J. Li, N-terminal mutant huntingtin associates with mitochondria and impairs mitochondrial trafficking, J. Neurosci. 28 (2008) 2783–2792.
[43] D.T. Chang, A.S. Honick, I.J. Reynolds, Mitochondrial trafficking to synapses in cultured primary cortical neurons, J. Neurosci. 26 (2006) 7035–7045.
[44] S. Chen, G.C. Owens, H. Makarenkova, D.B. Edelman, HDAC6 regulates mitochondrial transport in hippocampal neurons, PLoS One 5 (2010), e10848.
[45] X. Liu, D. Weaver, O. Shirihai, G. Hajnoczky, Mitochondrial 'kiss-and-run': interplay between mitochondrial motility and fusion–fission dynamics, EMBO J. 28 (2009) 3074–3089.
[46] M. Cagalinec, D. Safiulina, M. Liiv, J. Liiv, V. Choubey, P. Wareski, V. Veksler, A. Kaasik, Principles of the mitochondrial fusion and fission cycle in neurons, J. Cell Sci. 126 (2013) 2187–2197.
[47] V. Costa, M. Giacomello, R. Hudec, R. Lopreiato, G. Ermak, D. Lim, W. Malorni, K.J. Davies, E. Carafoli, L. Scorrano, Mitochondrial fission and cristae disruption increase the response of cell models of Huntington's disease to apoptotic stimuli, EMBO Mol. Med. 2 (2010) 490–503.
[48] X. Guo, M.H. Disatnik, M. Monbureau, M. Shamloo, D. Mochly-Rosen, X. Qi, Inhibition of mitochondrial fragmentation diminishes Huntington's disease-associated neurodegeneration, J. Clin. Invest. 123 (2013) 5371–5388.
[49] G. Twig, B. Hyde, O.S. Shirihai, Mitochondrial fusion, fission and autophagy as a quality control axis: the bioenergetic view, Biochim. Biophys. Acta 1777 (2008) 1092–1097.
[50] A. Jahani-Asl, M. Germain, R.S. Slack, Mitochondria: joining forces to thwart cell death, Biochim. Biophys. Acta 1802 (2010) 162–166.
[51] J.M. Oliveira, R.N. Lightowlers, Could successful (mitochondrial) networking help prevent Huntington's disease? EMBO Mol. Med. 2 (2010) 487–489.
[52] P.M. McLendon, B.S. Ferguson, H. Osinska, M.S. Bhuiyan, J. James, T.A. McKinsey, J. Robbins, Tubulin hyperacetylation is adaptive in cardiac proteotoxicity by promoting autophagy, Proc. Natl. Acad. Sci. U. S. A. 111 (2014) E5178–E5186.
[53] L. Zhang, C. Liu, J. Wu, J.J. Tao, X.L. Sui, Z.G. Yao, Y.F. Xu, L. Huang, H. Zhu, S.L. Sheng, C. Qin, Tubastatin A/ACY-1215 improves cognition in Alzheimer's disease transgenic mice, J. Alzheimers Dis. 41 (2014) 1193–1205.
[54] C. Geeraert, A. Ratier, S.G. Pfisterer, D. Perdiz, I. Cantaloube, A. Rouault, S. Pattingre, T. Proikas-Cezanne, P. Codogno, C. Pous, Starvation-induced hyperacetylation of tubulin is required for the stimulation of autophagy by nutrient deprivation, J. Biol. Chem. 285 (2010) 24184–24194.
[55] R. Xie, S. Nguyen, W.L. McKeehan, L. Liu, Acetylated microtubules are required for fusion of autophagosomes with lysosomes, BMC Cell Biol. 11 (2010) 89.
[56] C. Gonzalez, A. Couve, The axonal endoplasmic reticulum and protein trafficking: cellular bootlegging south of the soma, Semin. Cell Dev. Biol. 27 (2014) 23–31.
[57] Y. Wei, S. Pattingre, S. Sinha, M. Bassik, B. Levine, JNK1-mediated phosphorylation of Bcl-2 regulates starvation-induced autophagy, Mol. Cell 30 (2008) 678–688.
[58] M.M. Fu, J.J. Nirschl, E.L. Holzbaur, LC3 binding to the scaffolding protein JIP1 regulates processive dynein-driven transport of autophagosomes, Dev. Cell 29 (2014) 577–590.
[59] M. Arrasate, S. Mitra, E.S. Schweitzer, M.R. Segal, S. Finkbeiner, Inclusion body formation reduces levels of mutant huntingtin and the risk of neuronal death, Nature 431 (2004) 805–810.
[60] J. Miller, M. Arrasate, B.A. Shaby, S. Mitra, E. Masliah, S. Finkbeiner, Quantitative relationships between huntingtin levels, polyglutamine length, inclusion body formation, and neuronal death provide novel insight into Huntington's disease molecular pathogenesis, J. Neurosci. 30 (2010) 10541–10550.
[61] C.A. Gutekunst, S.H. Li, H. Yi, J.S. Mulroy, S. Kuemmerle, R. Jones, D. Rye, R.J. Ferrante, S.M. Hersch, X.J. Li, Nuclear and neuropil aggregates in Huntington's disease: relationship to neuropathology, J. Neurosci. 19 (1999) 2522–2534.
[62] B.E. Wade, C.E. Wang, S. Yan, K. Bhat, B. Huang, S. Li, X.J. Li, Ubiquitin-activating enzyme activity contributes to differential accumulation of mutant huntingtin in brain and peripheral tissues, J. Neurosci. 34 (2014) 8411–8422.
[63] Y. Kawaguchi, J.J. Kovacs, A. McLaurin, J.M. Vance, A. Ito, T.P. Yao, The deacetylase HDAC6 regulates aggresome formation and cell viability in response to misfolded protein stress, Cell 115 (2003) 727–738.
[64] C. Cook, T.F. Gendron, K. Scheffel, Y. Carlomagno, J. Dunmore, M. DeTure, L. Petrucelli, Loss of HDAC6, a novel CHIP substrate, alleviates abnormal tau accumulation, Hum. Mol. Genet. 21 (2012) 2936–2945.
[65] A. Bobrowska, P. Paganetti, P. Matthias, G.P. Bates, Hdac6 knock-out increases tubulin acetylation but does not modify disease progression in the R6/2 mouse model of Huntington's disease, PLoS One 6 (2011), e20696.
[66] B. Ravikumar, C. Vacher, Z. Berger, J.E. Davies, S. Luo, L.G. Oroz, F. Scaravilli, D.F. Easton, R. Duden, C.J. O'Kane, D.C. Rubinsztein, Inhibition of mTOR induces autophagy and reduces toxicity of polyglutamine expansions in fly and mouse models of Huntington disease, Nat. Genet. 36 (2004) 585–595.
[67] H. Jia, R.J. Kast, J.S. Steffan, E.A. Thomas, Selective histone deacetylase (HDAC) inhibition imparts beneficial effects in Huntington's disease mice: implications for the ubiquitin-proteasomal and autophagy systems, Hum. Mol. Genet. 21 (2012) 5280–5293.
[68] H. Jeong, F. Then, T.J. Melia Jr., J.R. Mazzulli, L. Cui, J.N. Savas, C. Voisine, P. Paganetti, N. Tanese, A.C. Hart, A. Yamamoto, D. Krainc, Acetylation targets mutant huntingtin to autophagosomes for degradation, Cell 137 (2009) 60–72.
[69] C. Rose, F.M. Menzies, M. Renna, A. Acevedo-Arozena, S. Corrochano, O. Sadiq, S.D. Brown, D.C. Rubinsztein, Rilmenidine attenuates toxicity of polyglutamine expansions in a mouse model of Huntington's disease, Hum. Mol. Genet. 19 (2010) 2144–2153.
[70] A.S. Tsvetkov, J. Miller, M. Arrasate, J.S. Wong, M.A. Pleiss, S. Finkbeiner, A small-molecule scaffold induces autophagy in primary neurons and protects against toxicity in a Huntington disease model, Proc. Natl. Acad. Sci. U. S. A. 107 (2010) 16982–16987.
[71] I. Taes, M. Timmers, N. Hersmus, A. Bento-Abreu, L. Van Den Bosch, P. Van Damme, J. Auwerx, W. Robberecht, Hdac6 deletion delays disease progression in the SOD1G93A mouse model of ALS, Hum. Mol. Genet. 22 (2013) 1783–1790.